J Intell Robot Syst (2010) 57:9–26
DOI 10.1007/s10846-009-9369-z

Accurate Modeling and Robust Hovering Control for a Quad–rotor VTOL Aircraft

Jinhyun Kim · Min-Sung Kang · Sangdeok Park

Received: 1 February 2009 / Accepted: 1 August 2009 / Published online: 17 September 2009

Abstract Quad-robot type (QRT) unmanned aerial vehicles (UAVs) have been developed for quick detection and observation of the circumstances under calamity environment such as indoor fire spots. The UAV is equipped with four propellers driven by each electric motor, an embedded controller, an Inertial Navigation System (INS) using three rate gyros and accelerometers, a CCD (Charge Coupled Device) camera with wireless communication transmitter for observation, and an ultrasonic range sensor for height control. Accurate modeling and robust flight control of QRT UAVs are mainly discussed in this work. Rigorous dynamic model of a QRT UAV is obtained both in the reference and body frame coordinate systems. A disturbance observer (DOB) based controller using the derived dynamic models is also proposed for robust hovering control. The control input induced by DOB is helpful to use simple equations of motion satisfying accurately derived dynamics. The developed hovering robot shows stable flying performances under the adoption of DOB and the vision based localization method. Although a model is incorrect, DOB method can design a controller by regarding the inaccurate part of the model

J. Kim
Department of Mechanical Engineering, Seoul National University of Technology,
Seoul, South Korea
e-mail: jinhyun@snut.ac.kr

M.-S. Kang
Department of Mechatronics Engineering, Hanyang University,
Ansan, South Korea
e-mail: wowmecha@gmail.com

S. Park (✉)
Division of Applied Robot Technology, Korea Institute of Industrial Technology,
Ansan, South Korea
e-mail: sdpark@kitech.re.kr

and sensor noises as disturbances. The UAV can also avoid obstacles using eight IR (Infrared) and four ultrasonic range sensors. This kind of micro UAV can be widely used in various calamity observation fields without danger of human beings under harmful environment. The experimental results show the performance of the proposed control algorithm.

Keywords Hovering control · QRT (quad-rotor type) UAV (unmanned aerial vehicle) · VTOL (vertical take-off and landing)

1 Introduction

Recently, researches on Unmanned Aerial Vehicles (UAVs) have been vigorously being performed for calamity observation such as woods and building fires, meteorological observation, patrol, and spraying agricultural chemicals to military purpose such as reconnaissance, monitoring, and communication etc. Moreover, the technology development of the UAVs is getting faster according to the rapid progress of electronic and computer technology. Micro UAVs can be operated on wide area regardless of the effect of ground configuration. The merit of UAVs is maximized for the practical use in the places where it is dangerous and difficult to approach. Further, micro UAVs are much cheaper and safer in dangerous tasks than piloted aircrafts.

Micro UAVs are classified into two categories, fixed and rotary wing types. The rotary wing type UAVs are more advantageous than the fixed wing type ones in the sense of VTOL(Vertical Take-off and Landing), omni-directional flying, and hovering performances. Rotary wing type UAVs are classified into quad-rotor type (QRT), co-axial helicopter, and helicopter etc. QRT UAVs have the simplest mechanical structure among them, and that is the reason why a QRT UAV is considered in this study as a flying platform.

QRT UAVs with various shape and size have been developed for commercial and research purposes, and some models are being sold as RC toys. Autonomous QRT UAVs equipped with high technology sensors are also being developed for special purposes, and researches for analysis and control of the flying robots are being done vigorously.

V. Mistler et al. derived the dynamic model for a four rotors helicopters, and developed a dynamic feedback controller [1]. P. McKerrow obtained the dynamic model for theoretical analysis of a dragonflyer [2]. A. Mokhtari and A. Benallegue obtained a nonlinear dynamic model of a QRT UAV for state variable control based on Euler angle and an open loop position state observer, emphasized attitude control rather than the translational motion of the UAV [3]. P. Castilo et al. performed autonomous take-off and hovering and landing control of a QRT UAV by synthesizing a controller using the Lagrangien model based on the Lyapunov analysis [4]. S. Bouabdallah et al. performed the design, dynamic modelling, sensing and control of an indoor micro QRT UAV [5]. S. Bouabdallah and R. Siegwart suggested two nonlinear control techniques: a backstepping and a sliding-mode control [6].

Flight control methods utilizing vision systems are also studied. E. Altuğ et al. proposed a visual feedback control method of a QRT UAV using a camera equipped on the UAV as the main sensor for attitude estimation [7]. T. Hamel et al. proposed a vision based visual servo controller for performing trajectory tracking tasks of under-actuated systems like QRT UAVs [8]. T. Hamel and R. Mahony proposed a vision based controller which performs visual servo control by positioning a camera onto a fixed target for the hovering of a QRT UAV [9].

Strictly speaking, earlier dynamic models are lack of mathematical rigorousness. They have dynamic inconsistency as they are expressed using both the reference and body coordinate systems without proper transformation [3, 6, 10–15]. This discrepancy mainly comes from the classical aerodynamic description based on the reference frame which is convenient in the case of using mechanical gyros, while the strip-down type gyros which are widely used in small QRT UAVs due to their compactness are much closer to describe the dynamic model using body frame coordinate system. Therefore, it is required to derive rigorous dynamic models of QRT UAVs both in the reference and body frame coordinate systems.

In the previous research, the linear and angular equations of motion is expressed in the reference frame and in the body frame coordinate, respectively. In some cases, they induced incorrect dynamic equations without consideration of the difference between two coordinates. [3, 6, 10–15]. In addition, for the controller, the angular equations of motion derived in the body frame coordinate is misused as the equations of motion derived in the reference frame without adequate assumptions.

In this paper, the above mentioned two problems will be solved. For the moving base system which is not fixed in an inertial frame, it is not convenient to derive the dynamic formulation using the Lagrangian in terms of the velocities expressed in a body-fixed frame. In UAV systems, the sensor information and actuator forces are exerted on a body-fixed frame, so it is more natural to write up the dynamics using body-fixed velocities. To supplement this, we used quasi-Lagrange approach [16]. The quasi-Lagrange method can give the equations of motion in terms of the body-fixed velocities. Finally the composite equations of motion for a QRT UAV will be derived strictly. In addition, using rigorous assumption–that is the roll and pitch angles are remain near zeros—the angular equations of motion derived in the body frame is induced the equations of motion in the reference frame. To guarantee the assumption, the robust controller based on disturbance observer(DOB) [17] is proposed. DOB is a kind of internal loop compensator which enforces desired nominal model on the original complex dynamic equations. The control input induced by DOB will be helpful to use simple equations of motion as mentioned above satisfying the accurate derived dynamics. In this work, rigorous dynamic models of a QRT UAV are obtained both in the reference and body frame coordinate systems. A disturbance observer(DOB) based controller using the derived dynamic models is also proposed for hovering control. And a vision based localization for the developed QRT UAV are introduced. The performance of the proposed control scheme is verified through experiments using QRT UAVs.

Section 2 shows the basic structure and the dynamics of the UAV. The DOB for flight control algorithms is given in Section 3. Section 4 shows the experimental setup and experimental results including the vision based localization schemes, and followed by concluding remarks in Section 5.

Fig. 1 Coordinate system

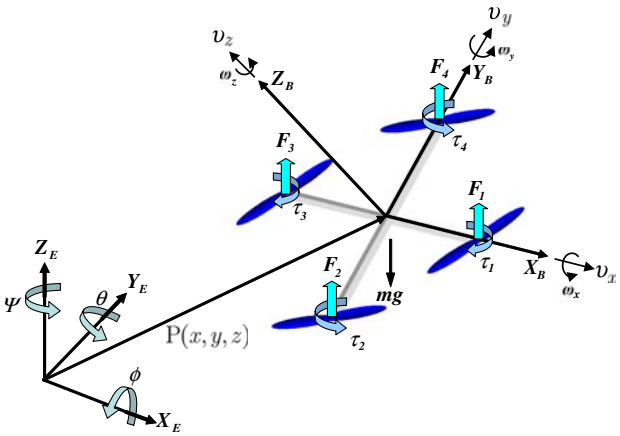

2 Dynamic Equations of Motion

Figure 1 shows coordinate systems of QRT UAVs. The motion of QRT UAVs is induced by the combination of quad rotors as shown in Fig. 2. The state vectors for the QRT UAVs are described as following:

$$\boldsymbol{\eta} = [\boldsymbol{\eta}_1^T, \boldsymbol{\eta}_2^T]^T;\ \boldsymbol{\eta}_1 = [x, y, z]^T; \quad \boldsymbol{\eta}_2 = [\phi, \theta, \psi]^T;$$
$$\boldsymbol{v} = [\boldsymbol{v}_1^T, \boldsymbol{v}_2^T]^T;\ \boldsymbol{v}_1 = [v_x, v_y, v_z]^T;\ \boldsymbol{v}_2 = [\omega_x, \omega_y, \omega_z]^T;$$

Fig. 2 QRT motion principle

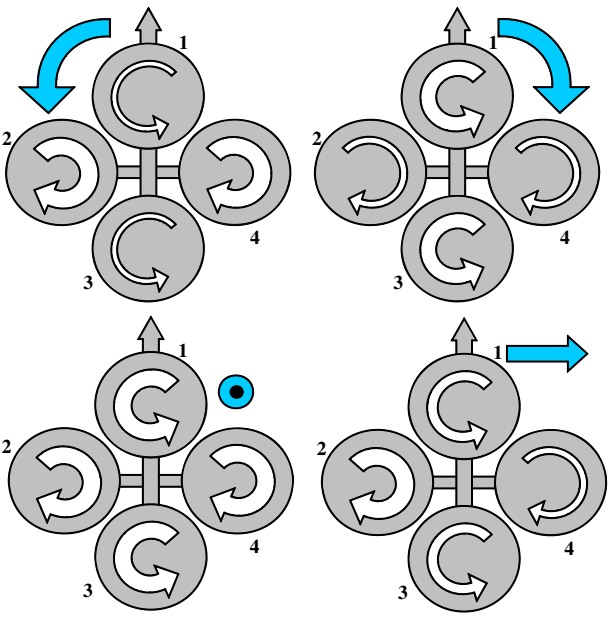

where the position and orientation of a QRT UAV, $\boldsymbol{\eta}$, are described relative to the inertial reference frame, while the linear and angular velocities of a QRT UAVs, $\boldsymbol{\nu}$, are expressed in the body-fixed frame. x, y, and z mean the linear positions of a QRT UAV with respect to inertial reference frame. ϕ, θ, and ψ represent the roll, pitch, and yaw angles of the QRT UAV in the inertial reference frame.

The inertial and body-fixed velocity relation can be represented with a QRT UAV Jacobian matrix [18].

$$\begin{bmatrix} \dot{\boldsymbol{\eta}}_1 \\ \dot{\boldsymbol{\eta}}_2 \end{bmatrix} = \begin{bmatrix} \mathbf{J}_1(\boldsymbol{\eta}_2) & \mathbf{0} \\ \mathbf{0} & \mathbf{J}_2(\boldsymbol{\eta}_2) \end{bmatrix} \begin{bmatrix} \boldsymbol{\nu}_1 \\ \boldsymbol{\nu}_2 \end{bmatrix} \Longleftrightarrow \dot{\boldsymbol{\eta}} = \mathbf{J}(\boldsymbol{\eta})\boldsymbol{\nu}, \tag{1}$$

where

$$\mathbf{J}_1(\boldsymbol{\eta}_2) = \begin{bmatrix} c\psi c\theta & -s\psi c\phi + c\psi s\theta s\phi & s\psi s\phi + c\psi c\phi s\theta \\ s\psi c\theta & c\psi c\phi + s\psi s\theta s\phi & -c\psi s\phi + s\theta s\psi c\phi \\ -s\theta & c\theta s\phi & c\theta c\phi \end{bmatrix}, \tag{2}$$

and

$$\mathbf{J}_2(\boldsymbol{\eta}_2) = \begin{bmatrix} 1 & s\phi t\theta & c\phi t\theta \\ 0 & c\phi & -s\phi \\ 0 & s\phi/c\theta & c\phi/c\theta \end{bmatrix}. \tag{3}$$

In above equations, $c(\cdot)$ and $s(\cdot)$ denote $\cos(\cdot)$ and $\sin(\cdot)$, respectively. Notice that $\mathbf{J}_2(\boldsymbol{\eta}_2)$ is undefined for a pitch angle of $\theta = \pm 90°$. However, in the QRT UAVs, the system goes into uncontrollable states as approaching the pitch angle. Hence, in this paper, we do not consider the pitch angle. In addition, $\mathbf{J}_2(\boldsymbol{\eta}_2)$ is not orthogonal matrix. Consequently, $\mathbf{J}_2^{-1}(\boldsymbol{\eta}_2) \neq \mathbf{J}_2^T(\boldsymbol{\eta}_2)$.

For the moving base system which is not fixed in an inertial frame, it is not convenient to derive the dynamic formulation using the Lagrangian in terms of the velocities expressed in a body-fixed frame. In QRT UAVs, the sensor information and actuator forces are exerted on a body-fixed frame, so it is more natural to write up the dynamics using body-fixed velocities. To supplement this, we used quasi-Lagrange approach [16]. The quasi-Lagrange method can give the equations of motion in terms of the body-fixed velocities.

2.1 Quasi-Lagrange Equations of Motion

The Lagrangian in general form is defined as

$$L = T - V, \tag{4}$$

$$T = \frac{1}{2}\boldsymbol{\nu}^T\mathbf{M}\boldsymbol{\nu} = \frac{1}{2}m\boldsymbol{\nu}_1^T\boldsymbol{\nu}_1 + \frac{1}{2}\boldsymbol{\nu}_2^T\mathbf{I}\boldsymbol{\nu}_2, \tag{5}$$

$$V = -mgz, \tag{6}$$

where m and $\mathbf{I}$ are mass and system inertia, respectively. Normally, we design the QRT UAV body as axisymmetric, so the inertia is defined as Eq. 7, and especially $I_{xx} = I_{yy}$.

$$\mathbf{I} = \begin{bmatrix} I_{xx} & 0 & 0 \\ 0 & I_{yy} & 0 \\ 0 & 0 & I_{zz} \end{bmatrix} \tag{7}$$

With the extended Hamiltonian principle, Eq. 4 gives following differential equations:

$$\frac{d}{dt}\left(\frac{\partial L}{\partial \boldsymbol{v}_1}\right) + \boldsymbol{v}_2 \times \frac{\partial L}{\partial \boldsymbol{v}_1} - \mathbf{J}_1^T \frac{\partial L}{\partial \boldsymbol{\eta}_1} = \boldsymbol{\tau}_1 \tag{8}$$

$$\frac{d}{dt}\left(\frac{\partial L}{\partial \boldsymbol{v}_2}\right) + \boldsymbol{v}_2 \times \frac{\partial L}{\partial \boldsymbol{v}_2} + \boldsymbol{v}_1 \times \frac{\partial L}{\partial \boldsymbol{v}_1} - \mathbf{J}_2^T \frac{\partial L}{\partial \boldsymbol{\eta}_2} = \boldsymbol{\tau}_2 \tag{9}$$

Then,

$$\mathbf{M}\dot{\boldsymbol{v}} + \mathbf{C}\boldsymbol{v} + \mathbf{g} = \boldsymbol{\tau}. \tag{10}$$

Finally, the 6 independent equations of motions are obtained as following:

$$m\left[\dot{v}_x - v_y\omega_z + v_z\omega_y - gs\theta\right] = 0, \tag{11}$$

$$m\left[\dot{v}_y - v_z\omega_x + v_x\omega_z + gc\theta s\phi\right] = 0, \tag{12}$$

$$m\left[\dot{v}_z - v_x\omega_y + v_y\omega_x + gc\theta c\phi\right] = u_1, \tag{13}$$

$$I_{xx}\dot{\omega}_x + \left(I_{zz} - I_{yy}\right)\omega_y\omega_z = u_2, \tag{14}$$

$$I_{yy}\dot{\omega}_y + \left(I_{xx} - I_{zz}\right)\omega_z\omega_x = u_3, \tag{15}$$

$$I_{zz}\dot{\omega}_z = u_4, \tag{16}$$

where

$$\boldsymbol{\tau} = \begin{bmatrix} 0 \\ 0 \\ u_1 \\ u_2 \\ u_3 \\ u_4 \end{bmatrix} = \begin{bmatrix} 0 \\ 0 \\ F_1 + F_2 + F_3 + F_4 \\ (-F_2 + F_4)l \\ (-F_1 + F_3)l \\ (-F_1 + F_2 - F_3 + F_4)\lambda \end{bmatrix}, \tag{17}$$

and l is the distance between the motor and the center of mass.

Equation 17 can be rewritten as the form of matrix like below:

$$\begin{bmatrix} u_1 \\ u_2 \\ u_3 \\ u_4 \end{bmatrix} = \begin{bmatrix} 1 & 1 & 1 & 1 \\ 0 & -l & 0 & l \\ -l & 0 & l & 0 \\ -\lambda & \lambda & -\lambda & \lambda \end{bmatrix} \begin{bmatrix} F_1 \\ F_2 \\ F_3 \\ F_4 \end{bmatrix} = \mathbf{T} \begin{bmatrix} F_1 \\ F_2 \\ F_3 \\ F_4 \end{bmatrix}. \tag{18}$$

2.2 Earth-Fixed Vector Representation

Until now, we derive the dynamic equation of motion related to the body fixed coordinate frame. However, for the control purpose, it is more convenient to use the dynamic equations derived in earth-fixed coordinate frame like below:

$$\mathbf{M}_\eta(\boldsymbol{\eta})\ddot{\boldsymbol{\eta}} + \mathbf{C}_\eta(\boldsymbol{v}, \boldsymbol{\eta})\dot{\boldsymbol{\eta}} + \mathbf{g}_\eta(\boldsymbol{\eta}) = \boldsymbol{\tau}_\eta(\boldsymbol{\eta}). \tag{19}$$

To express the dynamic equations in earth-fixed coordinate frame like Eq. 19, we need following relationship

$$\begin{aligned} \dot{\boldsymbol{\eta}} &= \mathbf{J}(\boldsymbol{\eta})\boldsymbol{v} && \Longleftrightarrow \boldsymbol{v} = \mathbf{J}^{-1}(\boldsymbol{\eta})\dot{\boldsymbol{\eta}} \\ \ddot{\boldsymbol{\eta}} &= \mathbf{J}(\boldsymbol{\eta})\dot{\boldsymbol{v}} + \dot{\mathbf{J}}(\boldsymbol{\eta})\boldsymbol{v} && \Longleftrightarrow \dot{\boldsymbol{v}} = \mathbf{J}^{-1}(\boldsymbol{\eta})[\ddot{\boldsymbol{\eta}} - \dot{\mathbf{J}}(\boldsymbol{\eta})\boldsymbol{v}] \end{aligned} \tag{20}$$

Then, the system matrices are defined as below:

$$\begin{aligned}\mathbf{M}_{\eta}(\boldsymbol{\eta}) &= \mathbf{J}^{-T}(\boldsymbol{\eta})\mathbf{M}\mathbf{J}^{-1}(\boldsymbol{\eta})\\ \mathbf{C}_{\eta}(\boldsymbol{\nu},\boldsymbol{\eta}) &= \frac{1}{2}\dot{\mathbf{M}}_{\eta}(\boldsymbol{\eta})\\ \mathbf{g}_{\eta}(\boldsymbol{\eta}) &= \mathbf{J}^{-T}(\boldsymbol{\eta})\mathbf{g}(\boldsymbol{\eta})\\ \boldsymbol{\tau}_{\eta}(\boldsymbol{\eta}) &= \mathbf{J}^{-T}(\boldsymbol{\eta})\boldsymbol{\tau}\end{aligned} \tag{21}$$

Finally, we can derive the equations of motion in earth-fixed coordinate frame.

$$m\ddot{x} = (s\psi s\phi + c\psi c\phi s\theta)u_1 \tag{22}$$

$$m\ddot{y} = (-c\psi s\phi + s\theta s\psi c\phi)u_1 \tag{23}$$

$$m(\ddot{z} + g) = c\theta c\phi u_1 \tag{24}$$

$$\mathbf{M}_{\eta_2}\ddot{\boldsymbol{\eta}}_2 + \frac{1}{2}\dot{\mathbf{M}}_{\eta_2}\dot{\boldsymbol{\eta}}_2 = \begin{bmatrix} u_2 \\ u_3 c\phi - u_4 s\phi \\ -u_2 s\theta + u_3 c\theta s\phi + u_4 c\theta c\phi \end{bmatrix} \tag{25}$$

where

$$\mathbf{M}_{\eta_2} = \begin{bmatrix} I_{xx} & 0 & -I_{xx}s\theta \\ 0 & I_{yy}c^2\phi + I_{zz}s^2\phi & (I_{yy} - I_{zz})c\phi c\theta s\phi \\ -I_{xx}s\theta & (I_{yy} - I_{zz})c\phi c\theta s\phi & I_{xx}s^2\theta + I_{yy}c^2\theta s^2\phi + I_z c^2\theta c^2\phi \end{bmatrix}. \tag{26}$$

2.3 Equations of Motion of a QRT UAV

As shown in previous subsections, the linear equations of motion of a QRT UAV are simple in earth-fixed reference frame, while the angular equations are advantageous to express in body-fixed reference frame. According to the above analysis, finally, the following equations are derived.

$$\begin{cases} m\ddot{x} = (s\psi s\phi + c\psi c\phi s\theta)u_1 \\ m\ddot{y} = (-c\psi s\phi + s\theta s\psi c\phi)u_1 \\ m(\ddot{z} + g) = c\theta c\phi u_1 \\ I_{xx}\dot{\omega}_x + (I_{zz} - I_{yy})\omega_y\omega_z = u_2, \\ I_{yy}\dot{\omega}_y + (I_{xx} - I_{zz})\omega_z\omega_x = u_3, \\ I_{zz}\dot{\omega}_z = u_4. \end{cases} \tag{27}$$

As shown in the Eq. 27, for the linear motions, all the states are subordinated to the control parameter u_1, hence only one state is controllable and the others are subjected to the controlled linear motion and angular motions. In this paper, for the hovering control, we only consider and control the $z-$directional linear motions.

Especially, the hovering control with $\phi \approx 0$ and $\theta \approx 0$ can make the dynamics much simpler form like Eq. 28, and it is easy to design the controller.

$$\begin{aligned} &m(\ddot{z} + g) = u_1 \\ &I_{xx}\ddot{\phi} = u_2 - (I_{zz} - I_{yy})\dot{\theta}\dot{\psi}, \\ &I_{yy}\ddot{\theta} = u_3 - (I_{xx} - I_{zz})\dot{\psi}\dot{\phi}, \\ &I_{zz}\ddot{\psi} = u_4. \end{aligned} \tag{28}$$

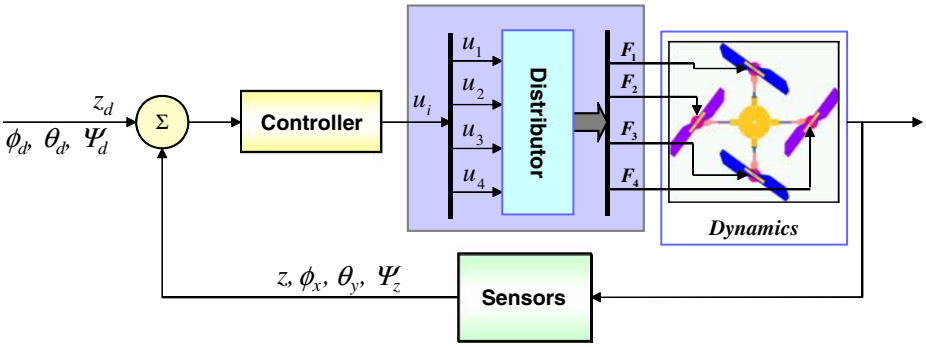

Fig. 3 Basic structure of the controller for the UAV

To satisfy the conditions where Eq. 28 is valid, ϕ and θ have to stay near the neutral positions, which are zeros. So, for the following section, the robust controller based on the disturbance observer for a QRT UAV is proposed.

3 Controller Design

Figure 3 shows the basic structure for the flight control of the UAV.

Now, let us consider following composite dynamic equations of motion.

$$\begin{bmatrix} m(\ddot{z}+g) \\ I_{xx}\ddot{\phi} \\ I_{yy}\ddot{\theta} \\ I_{zz}\ddot{\psi} \end{bmatrix} + \Delta = \begin{bmatrix} u_1 \\ u_2 \\ u_3 \\ u_4 \end{bmatrix}, \tag{29}$$

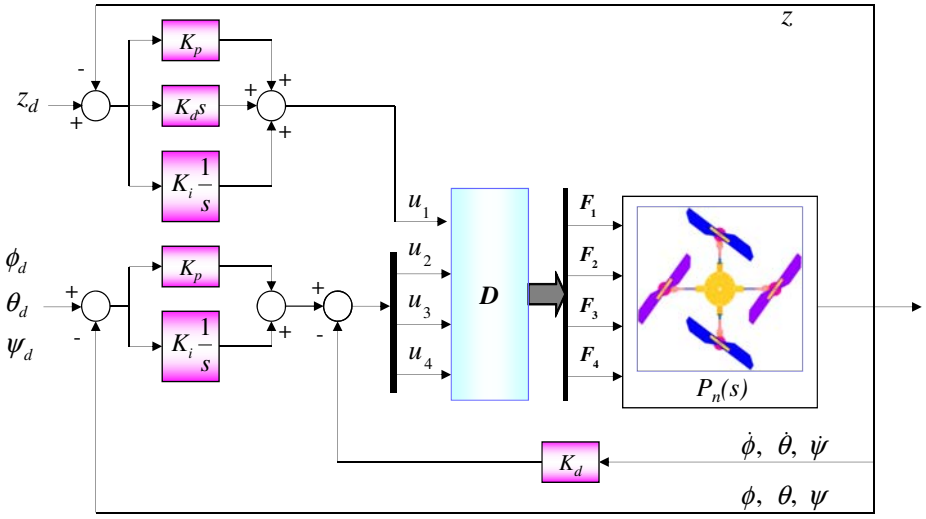

Fig. 4 PID controller for controlling the altitude and attitude of a QRT UAV

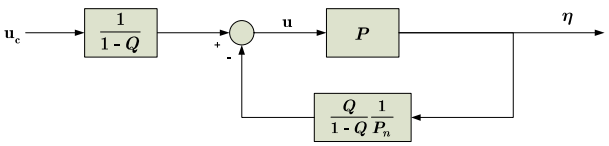

Fig. 5 Disturbance observer

where the disturbance, Δ, is defined as

$$\Delta = \begin{bmatrix} \delta_3 \\ \delta_4 + (I_{zz} - I_{yy})\omega_y\omega_z \\ \delta_5 + (I_{xx} - I_{zz})\omega_z\omega_x \\ \delta_6 \end{bmatrix}. \tag{30}$$

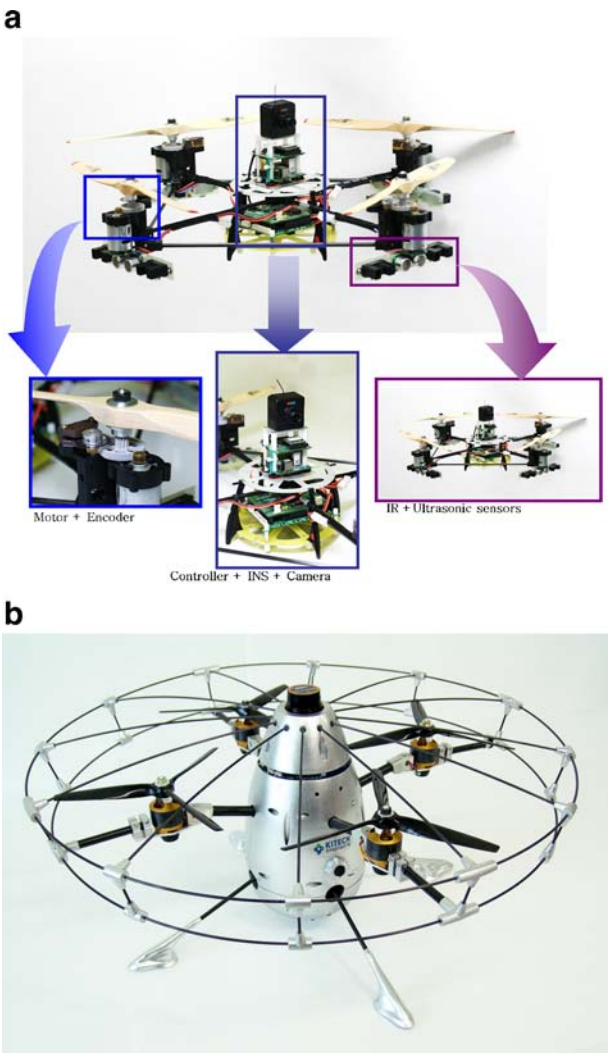

Fig. 6 The developed QRT Unmanned aerial vehicles.: **a** version 1; and, **b** version 2

Table 1 The specification and parameters of the QRT UAV version 2

Description	Value
Weight	2.2 kg
Diameter	573.6 mm
Height	170 mm
Distance between the motor and the C.G	172.5 mm
Propeller	$9'' \times 7''$
Moment of inertia in x-axis, I_{xx}	16.76337 gm^2
Moment of inertia in y-axis, I_{yy}	16.76337 gm^2
Moment of inertia in z-axis, I_{zz}	23.1447 gm^2

And δ_i mainly comes from the dynamic inconsistency. For the hovering control, the amount of disturbance is relatively small. Hence, it does not give instability, but poor performance, which may violate the assumption, $\phi \approx 0$ and $\theta \approx 0$. This phenomenon can be resolved using DOB control input.

3.1 Basic Controller

The control algorithms for the altitude and attitude, roll, pitch and yaw, of the UAV are designed based on PID controllers as shown in Fig. 4. The control input u_1 for controlling the altitude z of the UAV with respect to the reference input z_d is designed as

$$u_1 = K_{p1}(z_d - z) + K_{d1}\frac{\mathrm{d}(z_d - z)}{\mathrm{d}t} + K_{I1}\int_0^t (z_d - z)\mathrm{d}\tau. \tag{31}$$

The control inputs u_j ($j = 2, 3, 4$) for controlling the attitude (ϕ, θ, ψ) of the UAV with respect to the reference inputs $(\phi, \theta, \psi)_d$ are designed, respectively given as:

$$\begin{aligned} u_j = {} & K_{pj}\big[(\phi, \theta, \psi)_d - (\phi, \theta, \psi)\big] - K_{dj}(\dot{\phi}, \dot{\theta}, \dot{\psi}) \\ & + K_{I1}\int_0^t \big[(\phi, \theta, \psi)_d - (\phi, \theta, \psi)\big]\mathrm{d}\tau - \overline{u}_j. \end{aligned} \tag{32}$$

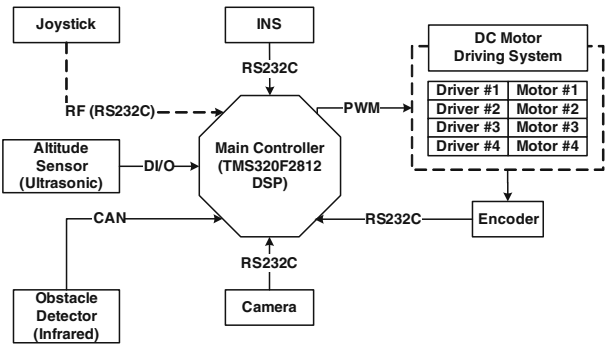

Fig. 7 Schematic view of the embedded controller

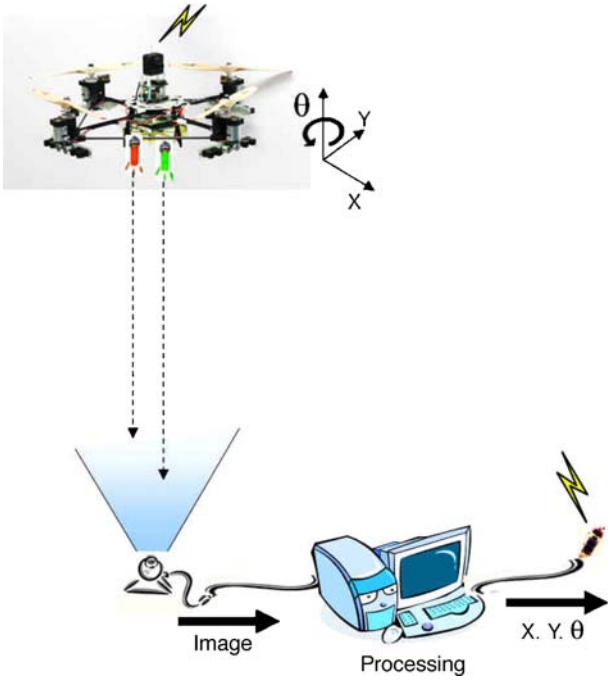

Fig. 8 The scheme of the vision based localization

$\overline{u}_j$ are the PD control inputs for avoiding obstacles in roll and pitch axis given as:

$$\begin{aligned}
\overline{u}_2 &= [K_{pr}(d_{rd} - d_r) - K_{dr}\dot{d}_r]U(d_{rd} - d_r) - [K_{pl}(d_{ld} - d_l) - K_{dl}\dot{d}_l]U(d_{ld} - d_l) \\
\overline{u}_3 &= [K_{pb}(d_{bd} - d_b) - K_{db}\dot{d}_b]U(d_{bd} - d_b) - [K_{pf}(d_{fd} - d_f) - K_{df}\dot{d}_f]U(d_{fd} - d_f) \\
\overline{u}_4 &= 0
\end{aligned} \tag{33}$$

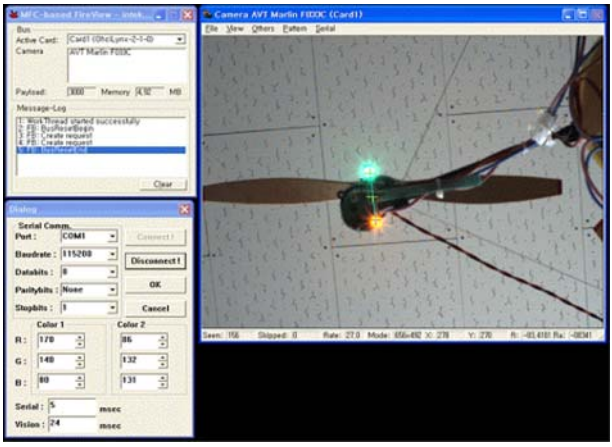

Fig. 9 The result of the vision based localization

Fig. 10 Experiments of the QRT Unmanned aerial vehicle

where d_{md} $(m = f, b, l, r)$ are reference distances for avoiding obstacles to forward, backward, left, and right direction, and d_m $(m = f, b, l, r)$ are distances of obstacles to the four direction. $U(d_{md} - d_m)$ $(m = f, b, l, r)$ are step functions as follows:

$$U(d_{md} - d_m) = \begin{cases} 1, & \text{for} \quad d_{md} < d_m \\ 0. & \text{for} \quad d_{md} > d_m \end{cases} \quad (m = f, b, l, r) \tag{34}$$

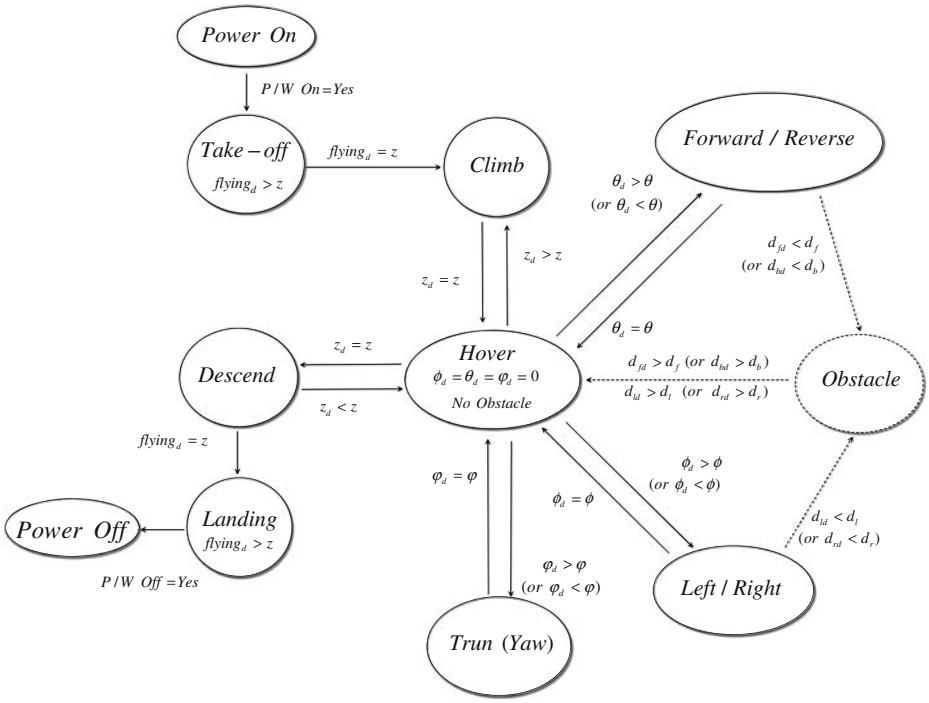

Fig. 11 The control flow of flying robot system

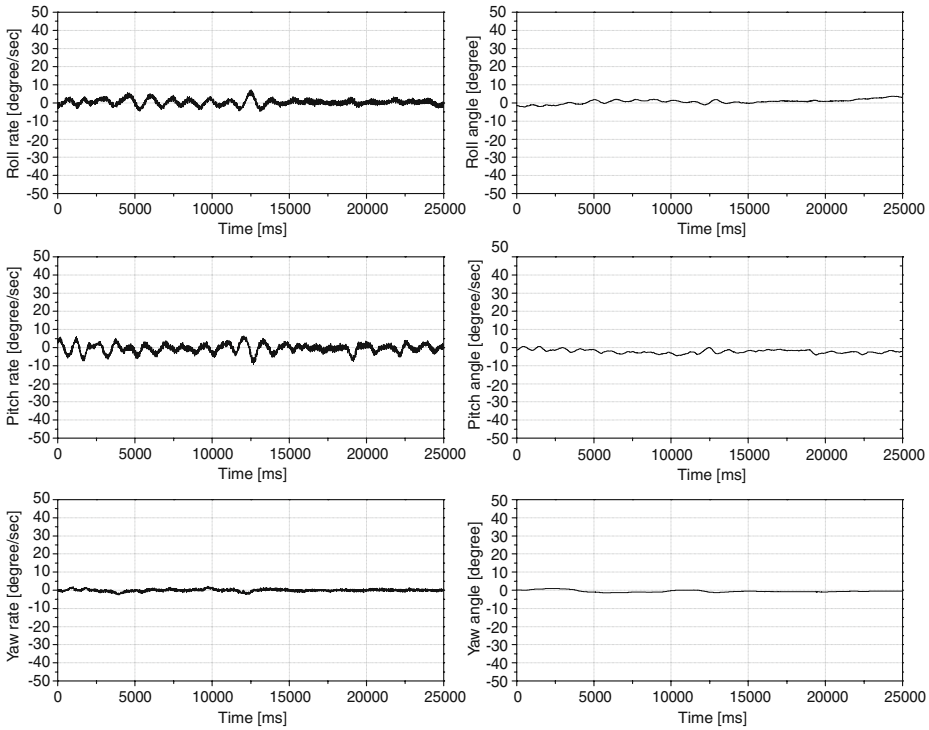

Fig. 12 Experimental results for hovering and attitude control of the developed UAV: hovering of the UAV

3.2 Disturbance Observer Based Disturbance Compensation

The control algorithms Eqs. 31 and 32 control the altitude and attitude of the UAV using sensor signals. The flight performance of the UAV, however, is not good in real flight because of the sensor noises and disturbances. The DOB based control algorithm, as shown in Fig. 5, controls the response of the plant $P(s)$ to follow that of the model plant $P_n(s)$ even though disturbances, sensor noise, and modeling uncertainty are applied to the plant.

Figure 5 shows the block diagram of disturbance observer. It can be expressed as

$$u(s) = \frac{1}{1-Q}u_c(s) - \frac{Q}{1-Q}\frac{1}{P_n}\eta(s). \tag{35}$$

DOB based disturbance compensator can be used to both for altitude and attitude control in the same way. In the cases the nominal models are given in the form of force-mass and inertia-moment dynamic models without friction, respectively given as $P_n = \frac{1}{ms^2}$ for the linear motion, and $P_n = \frac{1}{I_{xx,yy,zz}s^2}$ for the angular motion. And, for the Q-filter, we use well-known Q_{31} filter as following:

$$Q_{31}(s) = \frac{1+3\tau s}{(1+\tau s)^3}, \tag{36}$$

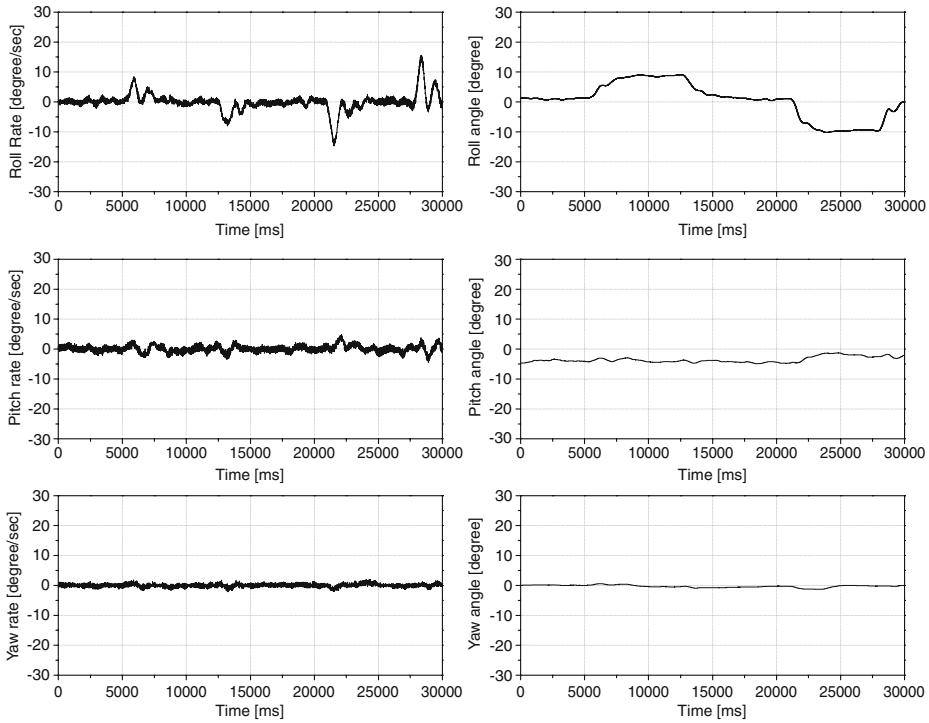

Fig. 13 Experimental results for hovering and attitude control of the developed UAV: desired roll angle of the UAV $= \pm 10^{\circ}$

Then, the internal loop will be conducted as

$$\begin{bmatrix} m(\ddot{z}+g) \\ I_x\ddot{\phi} \\ I_y\ddot{\theta} \\ I_z\ddot{\psi} \end{bmatrix} = \begin{bmatrix} u_{c1} \\ u_{c2} \\ u_{c3} \\ u_{c4} \end{bmatrix}. \tag{37}$$

Using Eq. 37, we can easily design the linear controller for each axis independently.

4 Experimental Results

4.1 Experimental Setup

Figure 6 shows the fabricated QRT UAVs for the purpose of calamity observation in indoor environment. The UAVs have 4 rigid blades driven by each BLDC motor mounted at each end of a crossing body frame. The Encoders for measuring speed are mounted on the motors. The UAVs are also equipped with an IMU(Inertial Measurement Unit) composed of three rate gyros for sensing attitude, eight IRs and four ultrasonic range sensors for obstacle detection, and one additional ultrasonic sensor for altitude measuring. A CCD camera with wireless RF(Radio Frequency) transmitter is mounted on the top of the UAV for the observation task. Table 1 gives

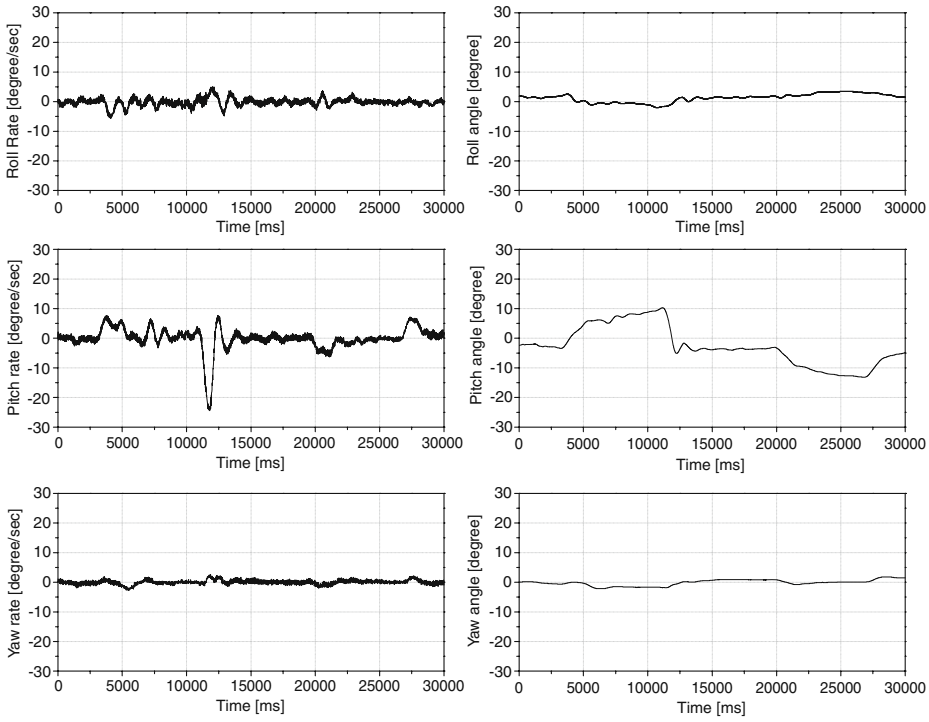

Fig. 14 Experimental results for hovering and attitude control of the developed UAV: desired pitch angle of the UAV $= \pm 10°$

the specification of the developed UAV. Figure 7 shows the schematic view of the embedded controller using a TMS320F2812 DSP controller.

4.2 Vision Based Localization

Figure 8 shows the scheme of the vision based localization. As the payload of the UAV is limited, red and green LED markers are attached at the bottom of the UAV, and a CCD camera is put on the ground. The CCD camera gets the image of the LED markers, and the image processor analyzes the color distribution of the markers, extract the center of each marker and finds the position and orientation of the markers as shown in Fig. 9 [19]. It takes 25ms for the image processing, and 5ms for serial communication.

4.3 Experiments and Results

Figure 10 shows the experiments of the hovering control of the QRT UAV.

Figure 11 shows the control flow of flying robot system. If detecting obstacles, the flying robot system avoids the obstacles by moving in the opposite direction. All flying movements except for takeoff states start on the hovering state, and if a certain movement is finished, it will be come back into the hovering state again.

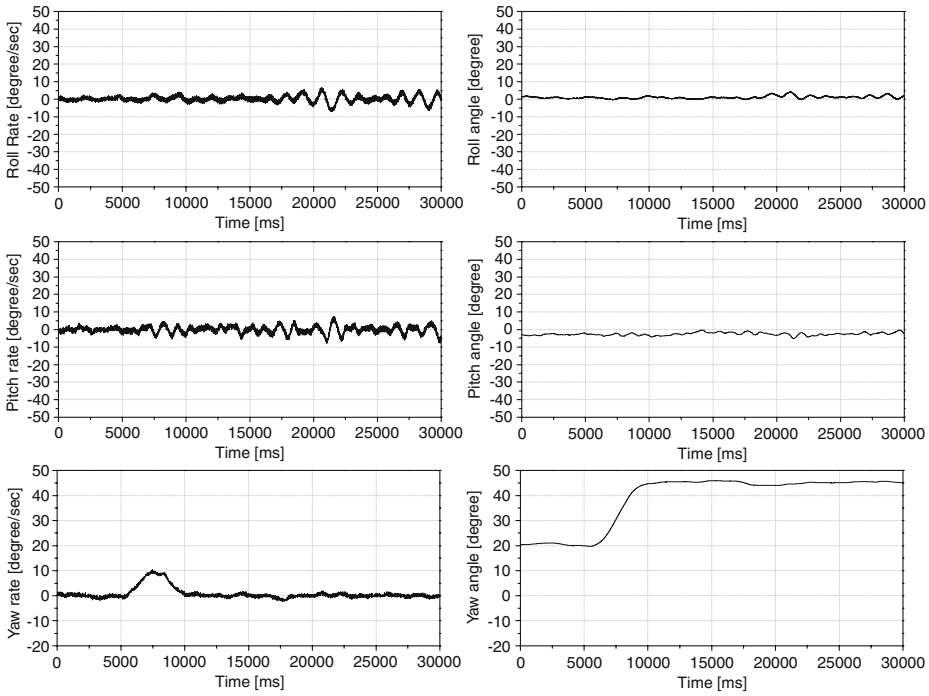

Fig. 15 Experimental results for hovering and attitude control of the developed UAV: desired yaw angle of the UAV = +45°

Figures 12, 13, 14, 15, 16 show the experimental results for hovering performance using attitude and altitude control. The left column of Fig. 12 shows roll, pitch, and yaw rates (up to down) and the right column shows roll, pitch, and yaw angles during hovering. Figures 13–15 show three angle rates and angles for pitch, roll, and yaw controls. As shown in the Fig. 16, the performance of the altitude control is very satisfactory, even though the sonar sensor is used. The results show that the proposed algorithm for both the altitude and attitude control of the UAV works well.

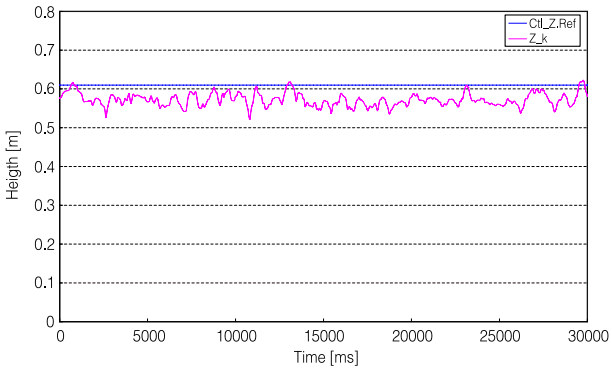

Fig. 16 Experimental results for hovering and altitude control of the developed UAV

For the hovering control, in this paper, a DOB controller with PID is proposed. With DOB, we can derive the linear equation, Eq. 37 using internal loop compensator, Eq. 36. As depicted in Fig. 4, a PID controller is used for the altitude and attitude of QRT UAVs. For the yaw controller, the I-gain is set to 0, because of the sensor noise. Normally the electrical compass is used for sensing the yaw motion, but the electrical compass is easily affected from other electrical systems, e.g., motor and battery.

5 Conclusion

In this study, a QRT UAV is developed for calamity observation in indoor environments. The hovering robot captures the image of targets under harmful environments, and sends the image to the operator on the safe site. The rigorous dynamic models of a QRT UAV were obtained both in the reference and body frame coordinate systems using the quasi-Lagrange equation. In many previous researches, they misused two subset motions as the whole body dynamics, however, at that case, the states of the whole body dynamics cannot be decoupled. A disturbance observer (DOB) based controller using the derived dynamic models was also proposed for hovering control and the vision based localization method. The control input induced by DOB will be helpful to use simple equations of motion satisfying the accurate derived dynamics. In addition, the UAV can also avoid obstacles using eight IR and four ultrasonic range sensors. The experiments were carried out to show the validity of the proposed control algorithm. The results show the attitude and height control results are very stable.

References

1. Mistler, V., Benallegue, A., M'Sirdi, N.: Exact linearization and noninteracting control of a 4 rotors helicopter via dynamic feedback. In: Proceedings of IEEE Intrnaltional Workshop on Robot and Human Interactive Communication, pp. 586–593 (2001)
2. McKerrow, P.: Modeling the draganflyer for-rotor helicopter. In: Proc., IEEE Int. Conf. on Robotics and Automation, pp. 3596–3601 (2004)
3. Mokhtari, A., Benallegue, A.: Dynamic feedback controller of euler angles and wind parameters estimation for a quadrotor unmmanned aerial vehicle. In: Proc., IEEE Int. Conf. on Robotics and Automation, pp. 2359–2366 (2004)
4. Castillo, P., Lozano, R., Dzul, A.: Stabilization of a mini-rotorcraft having four rotors. In: Proc., IEEE/RSJ Int. Conf. on Intelligent Robots and Systems, pp. 2693–2698 (2004)
5. Bouabdallah, S., Murrieri, P., Siegwart, R.: Design and control of an indoor micro quadrotor. In: Proc., IEEE Int. Conf. on Robotics and Automation, pp. 4393–4398 (2004)
6. Bouabdallah, S., Siegwart, R.: Backstepping and sliding-mode techmiques applied to an indoor micro quadrotor. In: Proc., IEEE Int. Conf. on Robotics and Automation, pp. 2259–2264 (2005)
7. Altuğ, E., Ostrowski, J., Mahony, R.: Control of a quadrotor helicopter using visual feedback. In: Proc., IEEE Int. Conf. on Robotics and Automation, pp. 72–77 (2002)
8. Hamel, T., Mahony, R., Chriette, A.: Visual servo trajectory tracking for a four rotor vtol aerial vehicle. In: Proc., IEEE Int. Conf. on Robotics and Automation, pp. 2781–2786 (2002)
9. Hamel, T., Mahony, R.: Pure 2d visual servo control for a class of under-actuated dynamic system. In: Proc., IEEE Int. Conf. on Robotics and Automation, pp. 2229–2235 (2004)
10. Castillo, P., Dzul, A., Lozano, R.: Real-time stabilization and tracking of a four-rotor mini rotorcraft. IEEE Trans. Control Syst. Technol. **12**(4), 510–516 (2004)
11. Guenard, N., Hamel, T., Moreau, V.: Dynamic modeling and intuitive control strategy for an x4-flyer. In: Proc. International Conf. on Control and Automation, pp. 141–146 (2005)

12. Kondak, K., Bernard, M., Meyer, N., Hommel, G.: Autonomously flying vtol-robots: modeling and control. In: Proc., IEEE Int. Conf. on Robotics and Automation, pp. 736–741 (2007)
13. Tayebi, A., McGilvray, S.: Attitude stabilization of a four-rotor aerial robot. In: Proc., IEEE Int. Conf. on Decision and Control, pp. 1216–1221 (2004)
14. Tayebi, A., McGilvray, S.: Attitude stabilization of a vtol quadrotor aircraft. IEEE Trans. Control Syst. Technol. **14**(3), 562–571 (2004)
15. Waslander, S., Hoffmann, G., Jang, J., Tomlin, C.: Multi-agent quadrotor testbed control design: integral sliding mode vs. reinforcement learning. In: Proc., IEEE/RSJ Int. Conf. on Intelligent Robots and Systems, pp. 468–473 (2005)
16. Meirovitch, L.: Dynamics and Control of Structures. Wiley, New York (1990)
17. Kaneko, K., Ohnishi, K., Komoriya, K.: A design method for manipulator control based on disturbance observer. In: Proc., IEEE/RSJ Int. Conf. on Intelligent Robots and Systems, pp. 1405–1412 (1994)
18. Fossen, T.I.: Guidance and Control of Ocean Vehicles. Wiley, New York (1994)
19. Yoon, K.-J., Jang, G.-J., Kim, S.-H., Kweon, I.-S.: Color landmark based self-localization for indoor mobile robots. J Control Autom Syst Eng **7**(9), 749–757 (2001)